Journal of Materials Chemistry C

Accepted Manuscript

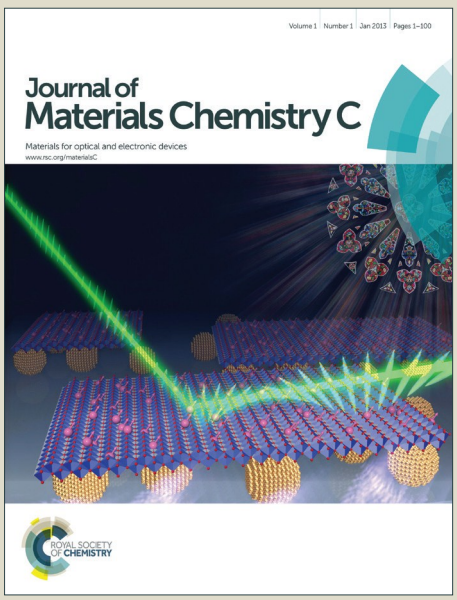

ROYAL SOCIETY OF CHEMISTRY

www.rsc.org/materialsC

Journal Name

COMMUNICATION

Modulating electrical conductivity of metal–organic framework films with intercalated guest π-systems

Received 00th January 20xx,
Accepted 00th January 20xx

DOI: 10.1039/x0xx00000x

www.rsc.org/

Zhiyong Guo,†[a] Dillip K. Panda,†[a] Krishnendu Maity,[a] David Lindsey,[a] T. Gannon Parker,[a] Thomas E. Albrecht-Schmitt,[a] Jorge L. Barreda-Esparza,[b] Peng Xiong,[b] Wei Zhou[c] and Sourav Saha*[a]

The access to electroactive metal–organic frameworks (MOFs) and the ability to manipulate their electrical properties with external stimuli are vital for the realization of MOF-based sensors and electronic devices. An electroactive blue MOF (BMOF) has been constructed using redox-active *N*,*N*′-bis(4-pyridyl)-2,6-dipyrrolidyl naphthalenediimide (BPDPNDI) pillars and 1,2,4,5-tetrakis-(4-carboxyphenyl)benzene (TCPB) struts. BMOF films grow selectively on ZnO-coated substrates under solvothermal conditions. Electrical conductivity of BMOF film is ca. 6×10^{-5} S/m (25 °C), which surges up to 2.3×10^{-3} S/m upon infiltration of π-acidic methyl viologen (MV^{2+}) guests, but remains unaffected by large C_{60} molecules, which are size excluded. These results demonstrate for the first time that the conductivity of MOFs can be fine-tuned by complementry guest π-systems that can promote long-range electron delocalization by forming extended π-stacks with the redox-active ligands.

Introduction

Owing to their innate ability to capture and concentrate guests selectively via size-exclusion, metal–organic frameworks[1] have emerged as powerful nanoscale containers that show great promise in a wide gamut of separation, storage, and delivery applications.[2–4] The evolution of MOFs as electronic, photonic, and magnetic materials, however, has been sluggish, in part because of the lack of sophisticated molecular recognition and signal transduction capabilities.[5] Furnishing these hybrid materials with redox- and photoactive building blocks should not only enrich them with intrinsic electronic and optical properties, but also enable them to communicate with and respond to various stimuli, such as guest entities, applied electric and magnetic fields, and light. Signals emanated from such interactions could then propagate through the extended networks, drawing new properties and functions that are non-native to the building blocks as well as the parent materials. Much of these possibilities, however, remain to be cultivated, but once realized, they should render MOFs capable of sensing,[5,6] electron transport,[8–11] and light harvesting,[12] and thereby expand their utility in batteries, transistors, and solar cells, among other molecular electronics devices.

Electrical conductivity has become one of the most sought after amenities in functional materials due in part to an increasing demand for energy efficient electrical devices. Although the ordered structures of MOFs apparently bode well for long-range charge transport and electrical conductivity, suggesting that they could eventually rival conducting polymers that suffer from structural defects and disorder, in reality, intrinsically conducting MOFs[9,10] are few and far between, and manipulating their electronic properties with external chemical and physical stimuli[11] remain extremely difficult tasks to achieve.

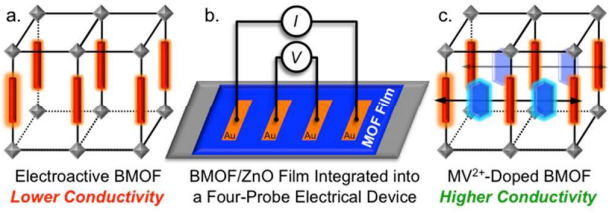

Fig. 1 Graphical illustrations of (a) an electroactive MOF made of redox-active ligands, (b) a four-probe electrical device composed of the electroactive MOF film grown selectively on a ZnO-coated surface, and (c) intercalation of π-acidic guests between the redox-active ligands leading to a better electron delocalization through the resulting π-D/A stacks and higher conductivity.

The factors that make it difficult to engineer electrical conductivity in MOFs include: (i) the scarcity of redox-active ligands that deprives MOFs of effective charge carriers and (ii) inadequate long-range charge delocalization caused by large separation between the ligands that restricts through-space electron movement and the σ-bonded metal clusters that prevent through-bond charge transport. One emerging strategy seeks to address these issues by developing planar[9] and columnar[10] MOFs, in which the redox-active building blocks can support long-range charge delocalization either via resonance or through the π-stacked ligands. Another approach exploits guest-induced oxidation of the built-in redox ceters[11] or crosslinking of nodes[12] to enhance the charge mobility. The success of these strategies notwithstanding, the former

[a] Department of Chemistry and Biochemistry, Florida State University Tallahassee, FL 32306, USA, E-mail: saha@chem.fsu.edu
[b] Department of Physics, Florida State University Tallahassee, FL 32306, USA.
[c] NIST Center for Neutron Scattering, National Institute of Standard and Technology, Gaithersburg, MD 20899, USA.
† Z.G. and D.K.P. contributed equally.
Electronic Supplementary Information (ESI) available: Experimental details, characterization, crystallographic data. See DOI: 10.1039/x0xx00000x

requires certain planar and columnar architectures that only a handful of ligands and metal ion nodes can afford,[9,10] whereas the node crosslinking strategy requires coordinatively unsaturated nodes, otherwise poses the risk of inflicting structural change due to ligand displacement.[13] Therefore, there exists the need for a general strategy that would give us access to electroactive MOFs and allow us to manipulate their conductivity with guests without disrupting their structures. The π-donor/acceptor interactions between redox-active ligands and complementary guests offer such opportunity, but they have yet to be exploited in MOFs for this purpose.

Furthermore, the successful integration and operation of MOFs in devices require stable, uniform, and electrically controllable films.[8,14] Most film growth protocols, however, are MOF specific, and do not necessarily afford suitable films for electrical measurements. For instance, the MOF films grown on insulating self-assembled monolayers (SAMs) are not particularly responsive to electrical fields, as SAMs impair electrical contact between MOFs and the underlying electrodes.[8] Promising electrochemical[15] and photochemical[16] deposition methods are emerging, but the question remains whether the redox- and photoactive ligands can withstand such invasive preparative conditions.

Results and Discussions

Addressing each of these critical challenges, in this all-encompassing work, we have (i) synthesized a new electro-active PPW-MOF, namely BMOF, using TCPB struts and redox-active BPDPNDI pillars (Fig. 1a), (ii) grown stable BMOF films under solvothermal conditions using ZnO-coated substrates (Fig. 1b), and (iii) demonstrated for the first time that the electrical conductivity of BMOF films can be fine-tuned by doping them with different π-acidic guests, such as MV^{2+}, dinitrotoluene (DNT), and 1,5-difluoro-2,4-dinitrobenzene (DFDNB) that can intercalate between the electron rich BPDPNDI pillars and thereby promote electron delocalization through the resulting π-stacks[17] (Fig. 1c).

Unlike unsubstituted NDIs, which are electron deficient colorless compounds, core-substituted NDIs (cNDIs)[18] possess tunable electronic, optical, and guest recognition properties that make them attractive building blocks of various functional materials. Although the simple NDI-based MOFs are not uncommon anymore,[7,19,20] the core-substituted NDI ligands have been rarely used in MOFs,[21] and their guest-induced optical and electrical responses have yet to be explored. Among cNDIs, the amine-tagged ones are the most electron rich, while bulky ligands are known to prevent catenation in PPW-MOFs.[20] On the basis of these facts, we envisioned that the BPDPNDI ligand adorned with two electron donating pyrrolidine pendants should not only endow BMOF with useful optoelectronic properties, but also yield a noncatenated architecture that can accommodate electroactive guests inside its cavities. BPDPNDI was synthesized (Scheme S1)[22] by installing two pyrrolidine rings on its naphthalene core via an S_NAr reaction,[18] followed by a Cu(II)-mediated coupling reaction[23] to introduce the pyridyl groups on the imide rings.

The navy-blue colored BMOF [Zn_2(TCPB)(BPDPNDI)] crystals were obtained from a reaction between $Zn(NO_3)_2.6H_2O$ (0.2 mmol), TCPB (0.1 mmol), and BPDPNDI (0.1 mmol) in DMF (10 mL) at 80 °C for 24 h (Fig. 2a).[20,22] The structure of BMOF was first solved partially from single-crystal X-ray (XRD) data, and then optimized by density functional theory calculations[22] to assign the atomic coordinates of the disordered pyrrolidine rings of BPDPNDI pillars. Overall, the noncatenated PPW architecture of BMOF (Fig. 2a) consists of TCPB-linked Zn_2 paddlewheel nodes located in the crystallographic *ab*-plane that are bridged by the BPDPNDI pillars aligned along the *c*-axis, making it isostructural to known [Zn_2(DBTCPB)(DPNDI)] (DBTCPB = dibromo-TCPB) MOF.[20a] The distances between the Zn_2-nodes—16, 11, and 19 Å along the *a*-, *b*-, and *c*-axes, respectively—are consistent with the lengths of the respective ligands. The simulated powder XRD (PXRD) pattern of BMOF conforms to that of the bulk material (Fig. 2b).

The PXRD studies further show that (Fig. S1) while the as-synthesized BMOF is highly crystalline, its crystallinity suffers after solvent evacuation but returns completely upon re-soaking in DMF. Such reversibility indicates that despite the loss of crystallinity, the structure and connectivity of evacuated BMOF remain intact under ambient conditions.

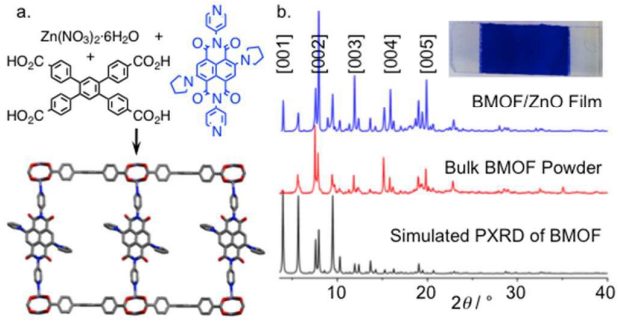

Fig. 2 (a) Solvothermal synthesis and crystal structure of noncatenated BMOF [Zn_2(TCPB)(BPDPNDI)]. (b) PXRD profiles of BMOF (simulated, powder, and film). Inset: Photograph of a blue BMOF/ZnO film.

Thermogravimetric analyses (Fig. S2) show that BMOF loses 70% of its initial weight at 120 °C due to DMF loss before decomposing at a much higher temperature (375 °C). The permanent porosity of BMOF is evident from its CO_2 adsorption capacity—65 cm^3/g at 273 K, 1 bar (Fig. S3)—which is comparable to that of isostructural [Zn_2(DBTCPB)(DPNDI)].[20a] The porous structure of BMOF bodes well for guest encapsulation and the subsequent guest-induced conductivity manipulation (*vide infra*).

Having constructed electroactive BMOF, we turned our attention to prepare its films for device integration and testing. Unable to grow BMOF films on glass, FTO, and ITO surfaces, we introduced annealed ZnO-coated substrates envisioning that the carboxylate struts can firmly anchor onto the ZnO surface and subsequently promote the formation of BMOF films.[24] The ZnO films were prepared by spin-coating FTO and bare glass slides with a ZnO/EtOH suspension, followed by sintering them at 350 °C for 0.5 h (Fig. 3a).[22] To

construct electrical devices, four Au electrodes (~100 nm thick) were vapor-deposited 1 mm apart on the ZnO-coated glass slides using patterned masks (Fig. 3b).[22] After initiating the formation of BMOF by heating DMF solutions of its precursors in screw-capped vials at 80 °C for 2 h, the ZnO-coated slides were immersed at upright positions and the entire setups were heated at constant 80 °C for different durations.[22] Within 1 h, only the ZnO coated areas became selectively covered with uniform BMOF films (Fig. 3b), which grew thicker with a longer immersion time, while the rest of the slides, including the Au-electrodes deposited on the ZnO layer remained completely BMOF-free. The BMOF films are stable in DMF, $MeNO_2$, MeCN, toluene, and other aprotic solvents, as well as when exposed to air under ambient conditions. The PXRD profiles of the blue films match nicely with that of bulk BMOF powder (Fig. 2b), confirming that the films are indeed composed of the surface-bound BMOF microcrystals.

The scanning electron microscopy (SEM) images show a uniform coverage of amorphous ZnO nanoparticles in bare ZnO films (Fig. 3c) and densely packed BMOF crystals covering the ZnO layer in BMOF/ZnO films (Fig. 3d). The cross-sectional (CS) SEM images (Fig. 3e) show that the annealed ZnO films are ca. 3 µm thick and the BMOF films grown on the ZnO films for 1 h are ca. 20 µm thick. The BMOF films remain mechanically stable and retain their crystalline morphology after becoming dry and being doped with different guests (Figures 3 and S4).

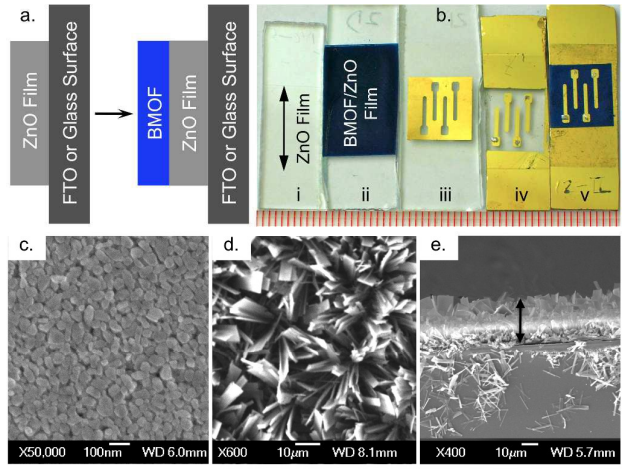

Fig. 3 (a) An illustration of selective growth of BMOF films on ZnO-coated substrates. (b) Photographs of (i) a transparent ZnO film, (ii) a BMOF film grown selectively on a ZnO film, (iii) a masked ZnO film, (iv) a ZnO device with four Au electrodes (1 mm apart), and (v) a BMOF/ZnO device equipped with Au electrodes. The SEM images of (c) ZnO and (d) BMOF films. (e) CS-SEM of a BMOF/ZnO film (BMOF 20 µm, ZnO 3 µm).

The BMOF films display (Fig. S5) strong visible absorption (λ_{max} = 615 nm) and redox properties (E_{Ox} = +920 mV, E_{Red} = –850 mV vs. Ag/AgCl) that coincide with those of the BPDPNDI ligands (λ_{max} = 610 nm; E_{Ox} = +880 mV, E_{Red} = –850 mV vs. Ag/AgCl).[22] The electrochemical studies of BMOF films grown on the ZnO-coated FTO electrodes suggest that, unlike insulating SAMs,[8] the ZnO layer provides sufficient electrical contact between the BMOF film and the underlying FTO electrode surface, making them electrically addressable.

Finally, to determine the electrical conductivity of BMOF films before and after infiltration of different guest π-systems, we measured the current-voltage (*I-V*) relationships (Figures 4a and S6) of the BMOF/ZnO devices quipped with four Au-electrodes.[22,25] Single crystal *I-V* measurement was not possible on small BMOF crystals, but the stable BMOF films allowed us to determine how their conductivity changes upon infiltration of different guests. The four-probe method not only eliminated the contact resistance that is typically imposed by two-probe pellet measurements,[22] but also circumvented the problems associated with using pellets in this particular study.[26] Since the BMOF (undoped and doped) and ZnO layers in BMOF/ZnO devices constitute two parallel connections between the Au electrodes, and charges can flow proportionately through both layers depending on their respective conductivities, the actual resistance of the BMOF films ($R_{component}$) was derived from the net resistances of the devices (R_{Device}) by extracting the resistance of the ZnO layer (R_{ZnO}) obtained from bare ZnO films using equation 1: $R_{component} = R_{Device} \cdot R_{ZnO} / (R_{ZnO} - R_{Device})$.[22] Then, from the resistance of each component, and taking probe-spacing (*d*), film thickness (*t*), and the lengths of Au electrodes (*l*) into account, electrical conductivity of the corresponding materials was calculated using equation 2: $\sigma_{component} = d / t \cdot l \cdot R_{component}$ (Table S1 and S2).[22] The net resistances of the ZnO and BMOF/ZnO devices are thickness-dependent, indicating that the charges actually move through the entire BMOF and ZnO films, not just their surfaces. Therefore, to ensure that the net resistances of the devices are consistent and reproducible, i.e., do not vary drastically from sample to sample (Tables S1, S2), the thickness of the ZnO films was maintained at 3 µm, and that of the BMOF films at 20 µm during their preparation.

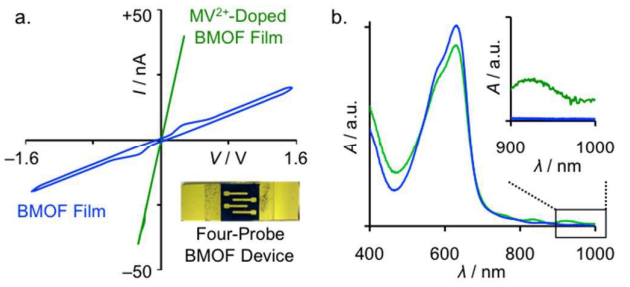

Fig. 4 (a) The *I-V* relationships of a BMOF/ZnO-glass devices (inset) before (blue line) and after (green line) doped with MV^{2+} for 70 h. (b) Vis-NIR spectra of a BMOF/ZnO film before (blue) and after (green) being doped with MV^{2+}. The latter shows new CT bands in the NIR region indicating π-donor/ acceptor CT interaction between BPDPNDI ligands and MV^{2+} guests.

The electrical conductivity of undoped BMOF films is ca. 6 × 10^{-5} S/m (25 °C), which is an order of magnitude greater than that of HKUST-1 that lacks redox-active ligands,[11d] but lower than that of intrinsically conducting planar and columnar networks.[9,10] The poor intrinsic conductivity of undoped BMOF films can be attributed to the lack of charge delocalization through the spatially separated BPDPNDI pillars. Crystal grain boundaries also diminish the conductivity of MOF films.[8] Nevertheless, owing to its porous structure adorned with

electron rich BPDPNDI pillars, the conductivity of BMOF films can be fine-tuned by infiltrating them with guest π-systems having appropriate size and electronic properties.

Envisioning that the intercalation of π-acidic guests between the electron rich BPDPNDI pillars could activate long-range electron delocalization through the resulting π-stacks, we immersed the BMOF devices into MV^{2+}, DFDNB, DNT, and C_{60} solutions and re-measured their *I-V* profiles under the same conditions (Table S1).[22] The conductivity of the BMOF films soaked in a MV^{2+} solution (30 mM/$MeNO_2$) increased gradually with the immersion time[22] before reaching the maximum at 2.3×10^{-3} S/m after 70 h of soaking (Fig. 4a), which corresponded to an impressive 35-fold upsurge from that of the undoped BMOF films. Similarly, the conductivities of the BMOF films soaked in less π-acidic DFDNB and DNT solutions (30 mM / $MeNO_2$) for 24 h reached the maximum levels at 3.5×10^{-4} and 1.5×10^{-4} S/m (Fig. S6),[22] respectively, representing modest six- and 2.5-fold improvements from the undoped BMOF films. On the other hand, the conductivity of BMOF films soaked in a C_{60} solution for 7 d remained practically unchanged (4×10^{-5} S/m), as the large C_{60} molecules (d = 11 Å) were size-excluded by BMOF. In the absence of BMOF films, the dip-coated dopant films show very high resistance that exceeds the detection limit of the source meter, which is consistent with the highly insulating nature of small aromatic compounds.

The fact that the stronger π-acidic guests (MV^{2+} > DFDNB > DNT) enhance the BMOF's conductivity more significantly than the weaker ones, suggests that the stronger donor/acceptor interactions forged by the former with the BPDPNDI ligands trigger more effective charge delocalization through the resulting π-stacks.[27] The ionic nature of MV^{2+} could also contribute in higher charge mobility in the MV^{2+}-doped BMOF films, while the size-excluded C_{60} had no noticeable impact on the BMOF's conductivity. Together, these results show that both size and the electronic properties of dopants dictate which ones are best suited for forming extended π-stacks with the electroactive ligands and enhancing their conductivity accordingly. This strategy can be applied to manipulate the electronic properties of other electroactive MOFs.

The conductivity of doped BMOF films after a quick wash with fresh solvents remain practically unchanged from that of the unwashed films, indicating that most of the encapsulated guest molecules stay inside BMOF.[22] However, after soaking the doped BMOF devices in solvents for prolonged time (72 h), their conductivities dropped close to that of the undoped BMOF films due to a gradual loss of dopants. Such reversibility is a unique and useful feature of this approach, which cannot be achieved with the coordinated guests that permanently change the structure and composition of parent MOFs.

The π-donor/acceptor interaction between the BPDPNDI pillars and the intercalated MV^{2+} guests was evident from the characteristic CT absorption band[7] in the NIR region displayed by the MV^{2+}-doped BMOF films (Fig. 4b). The influx of $MV^{2+}\cdot 2PF_6^-$ into BMOF was further confirmed through energy-dispersive X-ray spectroscopy (EDS), which revealed the diagnostic P and F signals in MV^{2+}-doped BMOF (Fig. S7). In BMOF, the gaps between the BPDPNDI ligands are such that more than one planar guest molecules can intercalate between them to form extended π-stacks, albeit not necessarily alternating donor/ acceptor stacks.

Conclusions

In summary, we have (i) constructed a new electroactive BMOF using an electron rich cNDI ligand, (ii) developed stable BMOF films on ZnO-coated substrates using a new protocol that could be adopted broadly to grow other MOF films, and (iii) devised a new strategy to fine-tune electrical conductivity of BMOF films by doping them with different π-acidic guests. The new film growth method should simplify device integration and testing of MOFs, while the ability to control the conductivity of MOFs with intercalated guests could expand their utility as sensors, semiconductors, and magnetic materials. Since electron transfer through π-donor/acceptor stacks can be harnessed by light,[28] light-harvesting and photoconducting MOFs could be realized. Ongoing studies in our laboratory and elsewhere probing at how different guests influence the optical and electronic properties of electroactive MOFs should pave the way for realizing MOF-based sensors and electronic devices in not too distant future.

Acknowledgements

This project was supported in part by American Chemical Society Petroleum Research Fund (51734-DNI4).

Notes and references

1 (a) T. R. Cook, Y.-R. Zheng and P. J. Stang, *Chem. Rev.,* 2012, **113**, 734–777; (b) H. Furukawa, K. E. Cordova, M. O'Keeffe and O. M. Yaghi, *Science,* 2013, **341**, 974–986.
2 (a) P. Nugent, Y. Belmabkhout, S. D. Burd, A. J. Cairns, R. Luebke, K. Forrest, T. Pham, S. Ma, B. Space, L. Wojtas, M. Eddaoudi and M. J. Zaworotko, *Nature* 2013, **495**, 80–84; (b) Y. He, W. Zhou, G. Qian and B. Chen, *Chem. Soc. Rev.,* 2014, **43**, 5657–5678.
3 P. Horcajada, R. Gref, T. Baati, P. K. Allan, G. Maurin, P. Couvreur, G. Férey, R. E. Morris and C. Serre, *Chem. Rev.,* 2012, **112**, 1232–1268.
4 (a) L. Ma, C. Abney and W. Lin, *Chem. Soc. Rev.,* 2009, **38**, 1248–1256; (b) M. Yoon, R. Srirambalaji and K. Kim, *Chem. Rev.* 2012, **112**, 1196–1231; (c) H. Fei and S. M. Cohen, *J. Am. Chem. Soc.,* 2015, **137**, 2191–2194.
5 (a) L. E. Kreno, K. Leong, O. K. Farha, M. Allendorf, R. P. Van Duyne and J. T. Hupp, *Chem. Rev.,* 2012, **112**, 1105-1125; (b) Z. Hu, B. J. Deibert and J. Li, *Chem. Soc. Rev.,* 2014, **43**, 5815-5840; (c) T.-H. Chen, I. Popov, W. Kaveevivitchai and O. S. Miljanic, *Chem. Mater.,* 2014, **26**, 4322–4325.
6 (a) Y. Takashima, V. M. Martínez, S. Furukawa, M. Kondo, S. Shimomura, H. Uehara, M. Nakahama, K. Sugimoto and S. Kitagawa, *Nat. Commun.,* 2011, **2**, 168; (b) S. Pramanik, Z. Hu, X. Zhang, C. Zheng, S. Kelly and J. Li, *Chem. Eur. J.,* 2013, **19**, 15964–15971; (c) A. Mallick, B. Garai, M. A. Addicoat, P. S. Petkov, T. Heine and R. Banerjee, *Chem. Sci.,* 2015, **6**, 1420–1425; (d) M. G. Campbell, D. Sheberla, S. F. Liu, T. M. Swager and M. Dincă, *Angew. Chem. Int. Ed.,* 2015, **54**, 4349–4352.

7 (a) B. D. McCarthy, E. R. Hontz, S. R. Yost, T. Van Voorhis and M. Dincă, *J. Phys. Chem. Lett.,* 2013, **4**, 453–458; (b) C. F. Leong, B. Chan, T. B. Faust and D. M. D'Alessandro, *Chem. Sci.,* 2014, **5**, 4724–4728.

8 (a) M. D. Allendorf, A. Schwartzberg, V. Stavila and A. A. Talin, *Chem. Eur. J.,* 2011, **17**, 11372–11388; (b) C. H. Hendon, A. Tiana and A. Walsh, Phys. *Chem. Chem. Phys.,* 2012, **14**, 13120–13132; (c) V. Stavila, A. A. Talin and M. D. Allendorf, *Chem. Soc. Rev.,* 2014, **43**, 5994–6010.

9 (a) S. Takaishi, M. Hosoda, T. Kajiwara, H. Miyasaka, M. Yamashita, Y. Nakanishi, Y. Kitagawa, K. Yamaguchi, A. Kobayashi and H. Kitagawa, *Inorg. Chem.,* 2009, **48***,* 9048–9050; (b) D. Sheberla, L. Sun, M. A. Blood-Forsythe, S. Er, C. R. Wade, C. K. Brozek, A. Aspuru-Guzik and M. Dincă, *J. Am. Chem. Soc.,* 2014, **136**, 8859–8862; (c) T. Kambe, R. Sakamoto, T. Kasumato, T. Pal, N. Fukui, K. Hoshiko, T. Shimojima, Z. Wang, T. Hirahara, K. Ishizaka, S. Hasegawa, F. Liu and H. Nishihara, *J. Am. Chem. Soc.,* 2014, **136***,* 14357–14360.

10 (a) T. C. Narayan, T. Miyakai, S. Seki and M. Dincă, *J. Am. Chem. Soc.,* 2012, **134**, 12932–12935; (b) S. S. Park, E.R. Hontz, L. Sun, C. H. Hendon, A. Walsh, T. Van Voorhis and M. Dincă, *J. Am. Chem. Soc.,* 2015, **137**, 1774–1777.

11 (a) Y. Kobayashi, B. Jacobs, M. D. Allendorf and J. R. Long, *Chem. Mater.,* 2010, **22**, 4120-4122; (b) M.-H. Zeng, Q.-X. Wang, Y.-X. Tan, S. Hu, H.-X. Zhao, L.-S. Long and M. Kurmoo, *J. Am. Chem. Soc.,* 2010, **132**, 2561–2563; (c) F. Gándara, F. J. Uribe-Romo, D. K. Britt, H. Furukawa, L. Lei, R. Cheng, X. Duan, M. O'Keeffe and O. M. Yaghi, *Chem. Eur. J.,* 2012, **18**, 10595–10601; (d) A. A. Talin, A. Centrone, A. C. Ford, M. E. Foster, V. Stavila, P. Haney, R. A. Kinney, V. Szalai, F. El Gabaly, H. P. Yoon, F. Léonard and M. D. Allendorf, *Science,* 2014, **343**, 66–69; (e) C. A. Farnandez, P. C. Martin, T. Schaef, M. E. Bowden, P. K. Thallapally, L. Dang, W. Xu, X. Chen and B. P. McGrail, *Sci. Rep.,* 2014, **4**:6114.

12 (a) A. Fateeva, P. A. Chater, C. P. Ireland, A. A. Tahir, Y. Z. Khimyak, P. V. Wiper, J. R. Darwent and M. J. Rosseinsky, *Angew. Chem. Int. Ed.,* 2012, **51**, 7440–7444; (b) T. Zhang and W. Lin, *Chem. Soc. Rev.,* 2014, **43**, 5982–5993; (c) M. C. So, G. P. Wiederrecht, J. E. Mondloch, J. T. Hupp and O. K. Farha, *Chem. Commun.,* 2015, **51**, 3501–3510; (d) J. Park, D. Feng, S. Yuan, H.-C. Zhou, *Angew. Chem. Int. Ed.,* 2015, ***55***, 430–435.

13 O. Karagiaridi, W. Bury, J. E. Mondloch, J. T. Hupp, O. K. Farha, *Angew. Chem. Int. Ed.,* 2014, **53**, 4530–4540.

14 (a) D. Zhacher, S. Rochus, C. Wöll and R. A. Fisher, *Angew. Chem. Int. Ed.,* 2011, **50**, 176–199; (b) O. Shekhah, J. Liu, R. A. Fischer and C. Wöll, *Chem. Soc. Rev.,* 2011, **40**, 1081–1106; (b) A. Bétard and R. A. Fischer, *Chem. Rev.,* 2012, **112**, 1055–1083;

15 I. Hod, W. Bury, D. M. Karlin, P. Deria, C.-W. Kung, M. J. Katz, M. So, B. Klahr, D. Jin, Y.-W. Chung, T. W. Odom, O. K. Farha and J. T. Hupp, *Adv. Mater.,* 2014, **26**, 6295–6300.

16 B. K. Keitz, C. J. Yu, J. R. Long and R. Ameloot, *Angew. Chem. Int. Ed.,* 2014, **53**, 5561–5565.

17 (a) R. S. Lokey, B. L. Iverson, *Nature* 1995, *375*, 303-305; b) C.R. Martinez, B.L. Iverson, *Chem. Sci.,* 2012, *3*, 2191-2201.

18 (a) C. Thalacker, C. Röger and F. Würthner, *J. Org. Chem.,* 2006, **71**, 8098–8105; (b) N. Sakai, J. Mareda, E. Vauthey and S. Matile, *Chem. Commun.,* 2010, **46**, 4225–4237; (c) S. Guha, F. S. Goodson, L. J. Corson and S. Saha, *J. Am. Chem. Soc.,* 2012, **134**, 13679–13691.

19 (a) M. Pan, X.-M. Lin, G.-B. Li, C.-Y. Su, *Coord. Chem. Rev.,* 2011, **255**, 1921–1936; (b) A. Mitra, C. T. Hubley, D. K. Panda, R. J. Clark and S. Saha, *Chem. Commun.,* 2013, **49**, 6629–6631.

20 (a) O. K. Farha, C. D. Malliakas, M. G. Kanatzidis and J. T. Hupp, *J. Am. Chem. Soc.* 2010, **132**, 950–952; b) W. Bury, D. Fairen-Jimenez, M. B. Lalonde, R. Q. Snurr, O. K. Farha and J. T. Hupp, *Chem. Mater.,* 2013, **25***,* 739–744.

21 C. R. Wade, M. Li and M. Dincă, *Angew. Chem. Int. Ed.,* 2013, ***52***, 13377–13381.

22 See ESI for details.

23 E. T. Chernick, M. J. Ahrens, K. A. Scheidt and M. R. Wasielewski, *J. Org. Chem.,* 2005, **70**, 1486–1489.

24 Y. Abdollahian, J. L. Hauser, I. R. Colinas, C. Agustin, A. S. Ichimura and S. R. J. Oliver, *Cryst. Growth Des.,* 2014, **14**, 1506–1509.

25 L. B. Valdes, *Proc. IRE, 1954*, ***42***, 420–427.

26 The BMOF pellets disintegrate easily when soaked in guest solutions. The packing densities of undoped and different doped BMOF in pellets are different. The contact resistances between the electrodes and undoped and doped BMOF pellets are not same either, but they can be neither quantified nor nullified by two-probe method. These factors render two-probe pellet measurements more error-prone and less suitable for the comparison of the conductivity of undoped and doped BMOF. Four-probe measurements on BMOF films circumvent or eliminate these issues, enabling a fair comparison.

27 The electron rich tetrathiafulvalene and *N*-methyl-phenothiazine compounds failed to enhance the conductivity of BMOF films, plausibly because their repulsive interaction with the electron rich BPDPNDI pillars hindered the formation of extended π-stacks needed for improved charge delocalization.

28 S. M. Mickley Conron, L. E. Shoer, A. L. Smeigh, A. B. Ricks and M. R. Wasielewski, *J. Phys. Chem. B,* 2013, **117**, 2195–2204.

Journal Name

COMMUNICATION

Graphical Abstract: